Geomechanics and Engineering, *Vol. 32, No. 6 (2023) 653-671*
https://doi.org/10.12989/gae.2023.32.6.653

Failure pattern of twin strip footings on geo-reinforced sand: Experimental and numerical study

Mahmoud Ghazavi[1a], Marzieh Norouzi[1b] and Pezhman Fazeli Dehkordi*[2]

[1]*Faculty of Civil Engineering, K.N. Toosi University of Technology, Tehran 19967-15433, Iran*
[2]*Department of Civil Engineering, Shahrekord Branch, Islamic Azad University, Shahrekord 88137-33395, Iran*

(*Received May 4, 2022, Revised February 25, 2023, Accepted February 27, 2023*)

Abstract. In practice, the interference influence caused by adjacent footings of structures on geo-reinforced loose soil has a considerable impact on their behavior. Thus, the goal of this study is to evaluate the behavior of two strip footings in close proximity on both geocell and geogrid reinforced soil with different reinforcement layers. Geocell was made from geogrid material used to compare the performance of cellular and planar reinforcement on the bearing pressure of twin footings. Extensive experimental tests have been performed to attain the optimum embedment depth and vertical distance between reinforcement layers. Particle image velocimetry (PIV) analysis has been conducted to monitor the deformation, tilting and movement of soil particles beneath and between twin footings. Results of tests and PIV technique were verified using finite element modeling (FEM) and the results of both PIV and FEM were used to utilize failure mechanisms and influenced shear strain around the loading region. The results show that the performance of twin footings on geocell-reinforced sand at allowable and ultimate settlement ranges are almost 4% and 25% greater than the same twin footings on the same geogrid-reinforced sand, respectively. By increasing the distance between twin footings, soil particle displacements become smaller than the settlement of the foundations.

Keywords: bearing pressure; failure mechanism; finite element modeling; geosynthetics; interfering strip footings; particle image velocimetry (PIV)

1. Introduction

In some practical cases, footings may be closely constructed such that they could tolerate heavy loads from superstructures. In such cases, the generated stress zones under the footings overlap leading to changing the bearing capacity mechanism, non-uniform settlements and tilt (Stuart 1962).

The impact of influencing factors on the bearing pressure of single isolated footings has been frequently reviewed in the literature (Ni Pengpeng *et al.* 2018, Mei *et al.* 2021). Besides, a comprehensive relevant review was presented to interference footings summarizing past studies to future prospects (Ghazavi and Fazeli Dehkordi 2021). Moreover, several researchers have studied the adjacency effect of strip footings using numerical and experimental methods (Das and Larbi-Cherif 1983a, b, Ghosh and Kumar 2011, Srinivasan and Ghosh 2013, Ghosh *et al*. 2015, Lavasan *et al*. 2018, Boufarh *et al*. 2019, Saha Roy and Deb 2018, Fazeli Dehkordi *et al*. 2019a, Schmüdderich *et al*. 2020a, b). These studies revealed that the bearing capacity of interfering footings increases with reduction space between footings and reaches the maximum value at certain spacing depending on soil characteristics, footing shape, and footing dimensions.

The enhancement of low strength soils under footings via polymeric reinforcements has been grown considerably in recent decades. It is more economical and faster to be installed than other techniques due to its significant confinement for the soil beneath footings, resulting in more stabilization and improvement in the bearing capacity and permanent settlement (Binquet and Lee 1975). Soil stabilization under interference footings using planar reinforcements can augment the bearing pressure and significantly reduce the tilt of footings (Kumar and Saran 2003, Ghazavi and Lavasan 2008, Ghosh and Kumar 2009, Javdanian *et al*. 2012, Lavasan and Ghazavi 2012, Naderi and Hataf 2014, Lavasan *et al*. 2017, Biswas and Ghosh 2018).

In recent years, it has been reported that 3-dimensional cellular reinforcements such as geocell, have successfully strengthened the loose soil (Rea and Mitchell 1978, Dash *et al*. 2003a, b, Sitharam and Sireesh 2006, Pokharel *et al*. 2010, Shadmand *et al*. 2018, Fazeli Dehkordi and Karim 2020, Fazeli Dehkordi *et al*. 2021a, b) especially for heavy-duty pavements and transportation infrastructure projects. Studies on single isolated footings on geocell-reinforced soils indicated that geocell could create additional confinements to the soil supporting footings resulting in a greater load carrying capacity (Han *et al*. 2008, Yang *et al*. 2010, Oliaei and Kouzegaran 2017, Arvin *et al*. 2021). In a recent review, all details regarding footing interaction on geo-reinforced soils are summarized (Fazeli Dehkordi *et al*. 2023).

Very few investigations have been accomplished on

*Corresponding author, Ph.D.
E-mail: p_fazeli@iaushk.ac.ir

ISSN: 2005-307X (Print), 2092-6219 (Online)

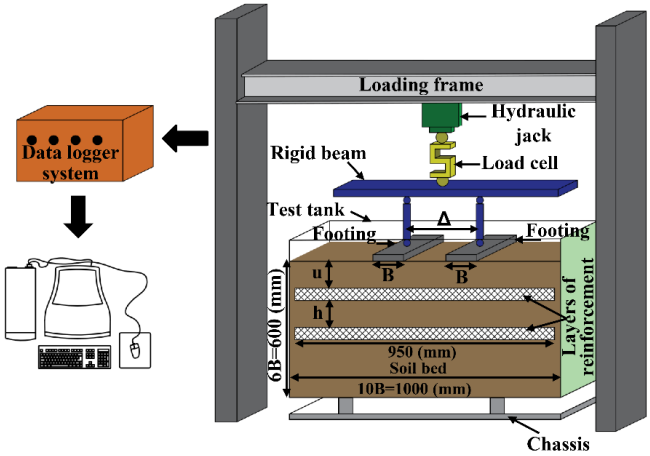

Fig. 1 Geometrical scheme and details of setup for interfering strip footings on geo-reinforced soil

cellular-reinforced soils to support twin footings. A study was conducted on two symmetric neighboring square foundations on geocell-reinforced clay using small-scale experiments (Gupta *et al*. 2018). After that, the influence of sand layer thickness was elucidated on the pressure-settlement response of twin circular footings using large-scale laboratory tests (Fazeli Dehkordi *et al*. 2019b). Besides, an additional factor was defined to classical bearing capacity solution for the effect of footings adjacency, reinforcement, and rigid base (Fazeli Dehkordi *et al*. 2021c, Fazeli Dehkordi 2022). A similar study was subsequently performed by numerical analysis on the basis of response surface technique (Ghazavi *et al*. 2023).

The review of the literature demonstrates that twin strip footings supported by geocell-reinforced soils have been received less attention. Thus, in the present report, the characteristics of two closely-spaced strip footings on geocell and geogrid-reinforced sand was investigated. The critical values for embedment depth and vertical spacing of reinforcements for individual and twin footings were proposed. An accurate image-based deformation measurement technique, called Particle Image Velocimetry (PIV), was utilized to monitor the soil deformation, settlement, and failure mechanism of the twin footings. To the best of the authors' knowledge, such an application has not been inquired deeply so far. A finite element modeling has been performed to verify model tests and confirm the failure mechanism of the footings.

2. Particle image velocimetry (PIV) technique

PIV method can be applied to measure the displacement and strain of the soil under footings. In this technique, digital images were taken during the loading process and the photos were then processed using GeoPIV8 software. This technique was initially developed at Cambridge University (White and Take 2002). The pioneering work of Adrian marked the beginning of an experimental study for fluid mechanics (Adrian 1991). Then, White *et al*. introduced a modified (White *et al*. 2003, O'loughlin and Lehane 2010) by using photography when the tests are performed, soil deformations could be visible in the considered plane. Obtaining displacement, axial and shear strain fields could be possible by taking, and comparing consecutive images at appointed times. PIV flow field processing system analyzes the displacement field of soil. With PIV, thousands of displacing points can be seen in one field of view. In addition, as a great advantage, the positions of these points can be determined after the tests are performed and at the desired points which optimize patches. In this research, Geo-PIV analysis was conducted with a patch size of 64×64 pixels with spacing equal to 32 pixels and 0.2mm/pixel of resolution. The standard error was also 0.0007 pixels. The results of experiments show good agreement with the results of numerical models, which indicates that, the PIV method can be used as a suitable method with high accuracy in geotechnical modeling. Therefore, prior researchers used PIV in their studies.

Employing the PIV to measure subsurface footing movements was obtained vertical displacement measurements at a Perspex-sand interface beneath a strip footing (O'loughlin and Lehane 2010). The effect of eccentricity load on settlement of shallow foundations resting on sandy soil models was investigated using PIV (Braim *et al*. 2016). Also, the impact of particle roundness and morphology on the shear failure mechanism of granular soil under a strip footing was studied using the PIV method to understand the soil-deformation mechanism (Ghalehjough *et al*. 2018). The capability of the PIV technique in determining the mixing ratio of two types of sand was demonstrated by conducting basic calibration tests (Miyamoto and Miyata 2020). The optical flow method measured the soil's small deformation in laboratory tests, and the results were validated with the PIV. That study shows that the displacement distribution deviates from commonly assumed linearity (Srokosz *et al*. 2021).

3. Test setup and procedure

3.1 Geometry of the test rig

A handmade setup was manufactured for model tests on

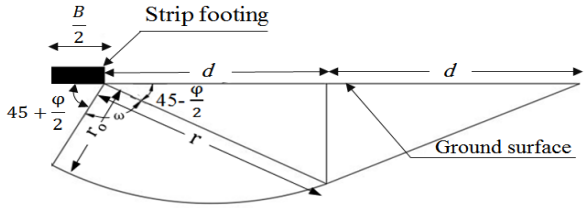

Fig. 2 General shear failure mechanism of the soil

single as well as two strip footings resting on unreinforced and geo-reinforced sand. The loading system comprises a rigid frame which was laid on a steel chassis. The height of the loading frame is 1600 mm comprising two stiff shafts and a horizontal rigid beam. The test tank is designed as a rigid steel box with 1000 mm length, 1000 mm height, and 520 mm width. The periphery of the box was strengthened with steel belts. The front side of the test box was built using a 20 mm thick transparent Perspex to supply transparent windows for perception. Fig. 1 shows the schematic representation of the test setup including the test box and steel frame.

According to Fig. 2, B is the foundation width, r and r_0 are shear surfaces and ω is equal to 90°. The amounts of r and r_0 for φ= 28 ° can be calculated from

$$r_o=\frac{B/2}{\cos(45+\frac{\varphi}{2})}=\frac{B/2}{\cos(45+\frac{28}{2})}=0.97B \quad (1)$$

$$r=r_o\, e^{\omega\tan\varphi}=2.16\ B \quad (2)$$

Thus, the length of horizontal vector of the failure surface (d) is

$$d=r\times\cos\left(45-\frac{28}{2}\right)=1.85\ B \quad (3)$$

Therefore, total width required for the box including spacing between footings can be computed as

$$L_{(\text{total width})}=4d+2B+0.6B=10B \quad (4)$$

($0.6B$ = The most distance spacing between footings)

In this study, the minimum size required for testing a tank based on the width of the footing (B=100 mm) is about 1000 mm. This dimension was also confirmed by preliminary numerical modeling by PLAXIS v20 software.

3.2 Model footing

The model footing made up of mild steel was used in the tests. The size of each twin strip footing was 100×520 mm with 20 mm thickness. A rasped orb which had no roughness with shaft was placed on each of the plates. Two U-shaped fasteners with two screw ends were used to fasten the retaining plate to the supporting beam. This was done to attach the load transfer system to the supporting beam as required to allow each of the brackets on the beam to move.

The task of the metal retaining plate was fixing the load transfer brackets on one hand and attaching the brackets to the support beam on the other hand. The end of the shaft was lubricated to avoid any friction. The bottoms of the footings placed at the soil surface were made rough by a thin coating layer of sand.

3.3 Loading system

The above-mentioned system was designed in such a way that all loads, displacements, and time values can be read and recorded automatically. A pre-calibrated load cell with 20 kN capacity was used and placed between the loading beam and rigid frame to precisely measure the pattern of the applied load on the trench surface. A pre-calibrated linear variable differential transducer (LVDT) with 0.01% accuracy was also placed on each of the footings to provide the soil surface settlement during the repeated load application. The displacement was applied continuously with a constant speed of 50 mm/h on the footing plates to achieve 50 mm settlement (S/B=50%) or reach the jack capacity, whichever occurred earlier. The ultimate bearing capacity of footings was measured at 10 mm settlement which is S/B=10% (Amar *et al*. 1994).

In order to investigate the impact of camera resolution on the accuracy of the PIV results, a Canon 700D with a resolution of 18 megapixels and a Canon 18-55 mm zoom lens were used. All controls such as focus, gain and shutter speed were adopted automatically. This arrangement is shown in Fig. 3. The testing system generally consists of five main parts namely loading system, testing tank, soil preparation device, data acquisition system and camera recording.

3.4 Backfill compaction

In order to provide experimental control and repeatability of the tests, the raining technique is utilized to deposit the soil in the test tank at a known and uniform density (Kolbsuzewski 1948). A moveable steel tank and a perforated steel plate are provided for raining the sand inside the test tank. It can be installed on the top of the test tank to pour the sand from a specified height. In order to obtain the required height for the desired density, a series of tests with different raining heights was performed. A raining height of 800 mm was used to reach 50% density which needs stabilization to tolerate heavy loads. As shown in Fig. 3, steel bars were welded on both sides of the tank, allowing the reinforcement to be embedded in the soil. A reinforcement layer (geogrid/geocell) with dimension of 950×520 mm was located in its situation and fixed with some temporary metal bars. For employing the geocell layer, it was stretched by the rebar at the top of leveled subgrade and filled with sand using sand raining technique with the same density. The test box walls were signed with lines having 100 mm intervals and the sand was rained with about 100 mm thickness. The accuracy of the sand placement and consistency of the placement density were checked during sand raining by placing small metal cans with known volumes at different locations in the box. Less than 4% deviation was observed among the measured densities at different levels in the box.

1. Thick transparent perspex
2. Camera
3. Remote of camera
4. Data logger
5. Oil pressure supply system for loading hydraulic jack
6. Test tank
7. Loading frame
8. Hydraulic jack
9. Footing plates
10. Loading transfer system
11. LVDT
12. Load cell

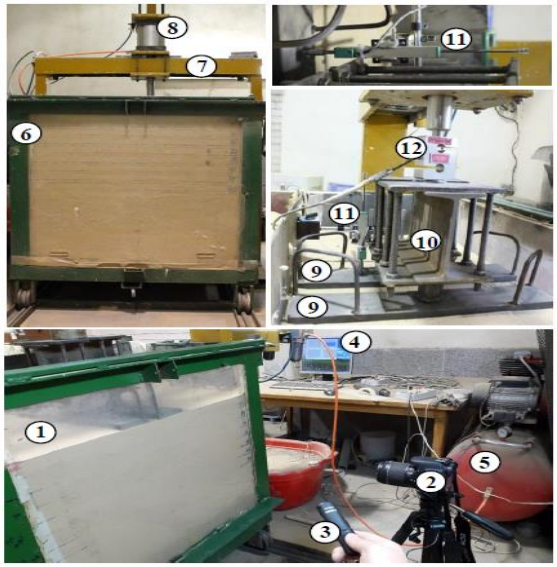

Fig. 3 Photographic view of the test box

Table 1 Detail of model tests performed in the current study

Type of footing	Type of reinforcement	Variables				No. of tests
		N	*u*/*B*	*h*/*B*	*Δ*/*B*	
Single	Unreinforced	-	-	-	-	1+1*
Single	Geocell-reinforced	1, 2	0.1, 0.2, 0.3	0.1	-	4+2*
Twin	Unreinforced	-	-	-	1.4, 1.6	2+1*
Twin	Geocell-reinforced	1, 2	0.1, 0.2, 0.3	0.1, 0.2	1.6	5+4*
Twin	Geocell-reinforced	1, 2	0.1	0.1	1.4	2+1*
Twin	Geocell-reinforced	1	0.1	-	1.2, 1.05	2+1*
Twin	Geogrid-reinforced	1, 2	0.1, 0.3, 0.5	0.3	1.6	4+2*

* The tests were conducted two times to verify the repeatability of the test data

3.5 Image analysis by PIV method

The digital images were analyzed using Geo-PIV software and by a MATLAB code (MATLAB R2007b). This code has been programmed and successfully used for geotechnical laboratory testing to measure deformations in soils (White *et al*. 2003). It has also been utilized to determine the deformations in frozen soils (Arenson *et al*. 2007). In this study, Geo-PIV was used to measure soil deformation. It is worth noting that Geo-PIV uses image texture to follow patches over a time series of pictures. Several patches were defined on the sample, and their movements were followed over time.

3.6 Testing programs

Several experiments were conducted to investigate the role of some influencing factors on the behavior of two neighboring strip foundations on the surface of geo-reinforced sand. These variables consist of the depth of the first reinforcement sheet from the base of the footings (u), the number of reinforcement layers (N), vertical space of two successive reinforcement layers (h) and distance between the center to center of footings (Δ). These are shown in Fig. 1.

The variables were considered as dimensionless forms as *u*/*B*, *h*/*B*, and *Δ*/*B* and the range of variables are displayed in Table 1. The amounts of reinforcement geometry, soil properties and footing dimension were deemed to be constant. Table 1 depicts the testing schedule for single and twin footings showing the number of repetitive tests in each series. The range of *u*/*B* and *h*/*B* in planar reinforcement was based on the previous studies recommending for twin footings supported by geogrid-reinforced soils (Ghazavi and Lavasan 2008, Javdanian *et al*. 2012). For 3-dimensional reinforcements, four values for *Δ*/*B* variable were assumed

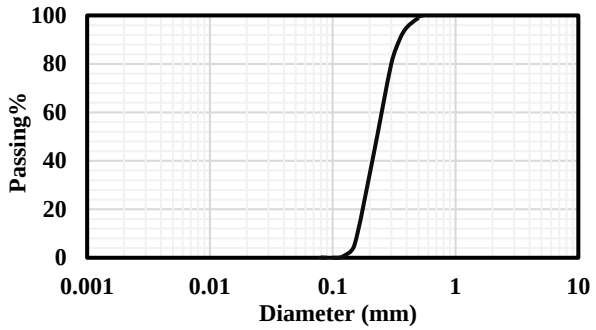

Fig. 4 Grain size distribution for sand used in present study

Table 2 Physical properties of soil used in the present study

Property	Value
$D_{10\ (mm)}$	0.16
$D_{50\ (mm)}$	0.27
$D_{60\ (mm)}$	0.28
C_u	1.88
C_c	0.87
e_{max}	0.94
e_{min}	0.54
γ_d (kN/m^3)	15.7
G_s	2.62
Friction angle at D_r=50%	28°
Elasticity modulus (MPa) at D_r=50%	20

with respect to the test box to avoid boundary effects. For geogrid-reinforced cases, the value of Δ/B was taken 1.6 to reach the maximum bearing pressure on geogrid-reinforced sand (Ghazavi and Lavasan 2008). As a whole, 30 experiments including repetitive tests were performed in the study.

4. Test materials

4.1 Soils

The sand used is the well-known Firoozkooh sand (No. 161), commercially available from Firoozkooh mine in the northeast of Tehran. The size distribution of the sand is shown in Fig. 4. The soil is SP according to the Unified Soil Classification System (USCS) (ASTM D 2478). The soil exploited in this investigation was dry sand and relatively uniform. Table 2 represents the properties of the sand according to ASTM standards. The internal friction angle of the sand (φ) at relative compaction of 50% and the elasticity modulus (E_s) of the subgrade were examined employing average results of three drained triaxial tests (ASTM D 7181).

4.2 Reinforcement

In this study, both planar (e.g., geogrid) and 3-dimensional cellular (e.g., geocell) reinforcements were used for experiments. To reduce the scale effect, a weak commercial geogrid with small aperture size, as mentioned in Table 3, was employed as planar reinforcement (Milligan *et al*. 1986, Adams and Collin 1997). Load-deformation test was performed according to ASTM D6637 on the geogrid in both machine direction and cross machine direction to determine the tensile resistance of reinforcement.

Table 3 Engineering properties of reinforcements

Type	Description	Value
Geogrid	Polymer	HDPE
	Thickness (mm)	2.2
	Ultimate tensile strength (kN/m)	6
	Aperture size (mm)	10×10
	Mass per unit area (gr/m^2)	700
Geocell	Polymer	HDPE
	Thickness (mm)	2.2
	Ultimate tensile strength (kN/m)	6
	Aperture size (mm)	50×50
	Cell wall height (mm)	50
	Mass per unit area (gr/m^2)	1120
Joints	Material	Nylon
	Color	White
	Length (mm)	50
	Ultimate tensile strength (Mpa)	2.8

To compare the efficiency of 3-dimensional reinforcement with planar reinforcement, a geocell layer was also fabricated from the same geogrid material (Fig. 5). The geocell layers were prepared by cutting geogrid pieces to the required length and height from full rolls and creating pre-specified dimensions. The honeycomb shape of geocell was created by placing the pieces in transverse and diagonal directions and jointing together using nylon cable ties. In each joint, three ties are utilized at the top, middle and bottom of gecell wall (see Fig. 5(c)). The joint strength of the geocell was examined by measuring the resistance of a nylon cable tie. The joint strength would be three times the resistance of each cable because having three cable ties at each joint. Three cable ties used in each joint brought more tensile strength than the resistance of geogrid material. Thus, any failure in the geocell sheet happens in the material reinforcement similar to geogrid reinforcement. It is worth mentioning here that the material consumed to make geocell is almost 1.6 times more than that used for geogrid of the same plan area. As a result, the variation of bearing pressure due to the geometric shape and weight of reinforcement material used can be estimated.

The produced pocket sizes of geocell were 50×50×50 mm^3 (lenght×width×height). The dimensions of these cells were such that the loading plate as a footing covers many cells (B=100 mm), tending to get the results closer to reality. It is noteworthy here that, bigger geocell pocket relative to the footing width may lead to local (punching effect) for the footings. Besides, increase in the pocket size leads to reduction of the soil confinement under footings and reinforcement benefits (Rajagopal *et al.* 1999). The properties of the geocell are also given in Table 3.

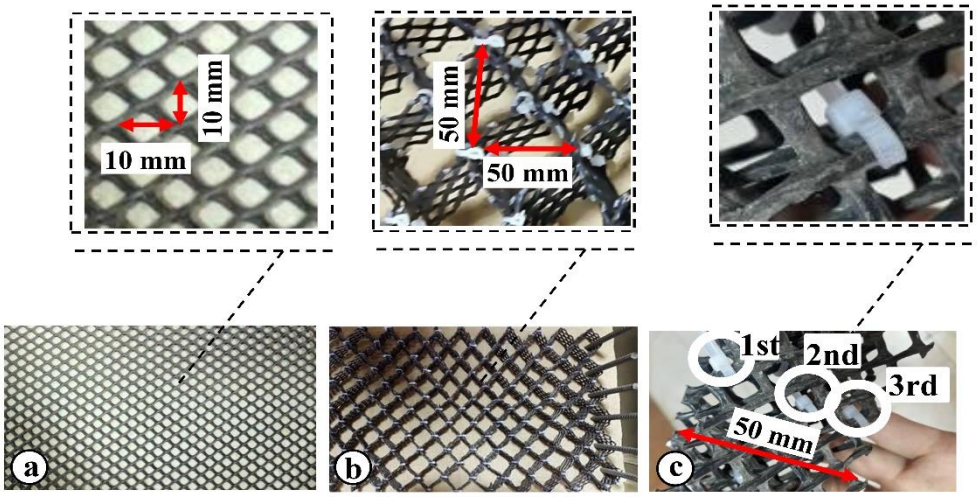

Fig. 5 Photographic view of a (a) geogrid layer, (b) geocell layer fixed in place by the rebar and (c) geocell layer before expanded

5. Results and discussion

In the model tests, the number of reinforcements and their vertical distance were varied while other reinforcement conditions were kept constant. A series of model tests was performed to study the effect of changing the number and the vertical spacing of reinforcement layers on the performance of the reinforced soil supporting footings. Another series of model tests was also performed to study the influence of footing interference on reinforced sand with changing center to center distance of the footings.

5.1 Single footing

According to Fig. 6 showing measurements of LVDT, the variation of the footing bearing pressure on unreinforced as well as geocell-reinforced soil against settlement for changing u and h could be harvested. Increasing u/B and h/B values beyond optimum amounts caused a decrease of the bearing capacity of the foundation. According to the obtained results, the most suitable depth for geocell placement is $0.1B$, similar to observations of former studies (Dash *et al*. 2001, Bush *et al*. 1990). Besides, increasing the number of geocell layers (N) reduces the footing settlement due to more confinement and stiffness of the soil beneath the footing. It should be mentioned that the reinforcements caused by the soil could sustain more pressure and settlement, witnessing no failure limit. As suggested by a former study, the value of h/B is considered similar to u/B in all cases (Ghazavi and Lavasan 2008). Prior studies recommended the optimum buried depth and its spacing for planar reinforcement supported individual footing is almost $u/B=h/b=0.3$ (Yoo 2001, Abu-Farsakh *et al*. 2007). Thus, these two values were assumed as optimum amounts for individual footing on planar-reinforced soil.

5.2 Twin footings

5.2.1 The effect of embedment depth and spacing reinforcement layers

Fig. 6(b) depicting results of measurements from LVDT clearly shows the effect of embedment depth of cellular and planar reinforcements on the load-carrying capacity of two interacting footings $\Delta/B=1.6$ spacing. As observed, the geocell layer increases the footing bearing pressure more than geogrid. This is because geocell makes better status than geogrid due to generating additional confinement in the subsoil, leading to enhanced footing bearing pressure.

According to the results of Fig. 6(b), the best ratio for embedment depth of the geogrid and geocell reinforcement to achieve the maximum bearing capacity of two interacting footings are $(u/B)_{cr}=0.1$ and 0.3, respectively.

Fig. 6(b) also displays the variation of bearing pressure at different numbers of reinforcements for $\Delta/B=1.6$. As shown, for a given settlement, reinforcement layers provided additional footing bearing pressure. Furthermore, for a specific applied load on the footings, the settlement ratio decreases with increasing the number of reinforcement layers because more reinforcement significantly increases the stiffness of the reinforced sand bed. However, by increasing the number of reinforcing layers, less significant effect was seen on improving the soil behavior. The improvement of bearing pressure with one layer of geocell reinforcement is more prominent than that obtained with two geogrid layers. This means that increasing solely geogrid layers may not improve the bearing pressure markedly. An effective way to make good progress is changing planar reinforcement to geocell reinforcement. These comparisons show that increasing reinforcement layers cause no drastic decline in the settlement. When the number of the geogrid and geocell layers increases to two layers, the bearing capacity of the foundation increases only 3 and 4 percent at the ultimate settlement ratio of $S/B=10\%$, respectively. In general, the use of geocell for soil reinforcement is an effective solution for enhancement of load-carrying characteristics of foundations due to three-dimensional structure of geocell.

No effective changes take place in the bearing capacity of footings on reinforced soil at allowable settlement lower than $S/B=2\%$. Such changes occur beyond failure

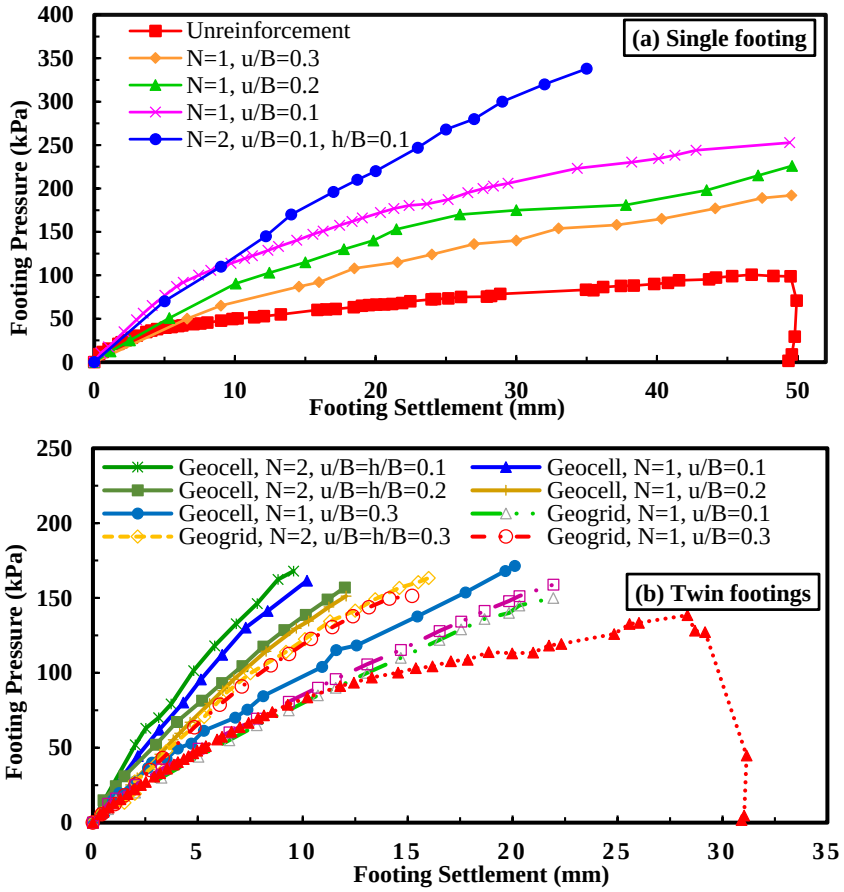

Fig. 6 Load-settlement variation from LVDT for unreinforced soil and geocell-reinforced sand supported: (a) single footing and (b) interfering footings (Δ/B=1.6)

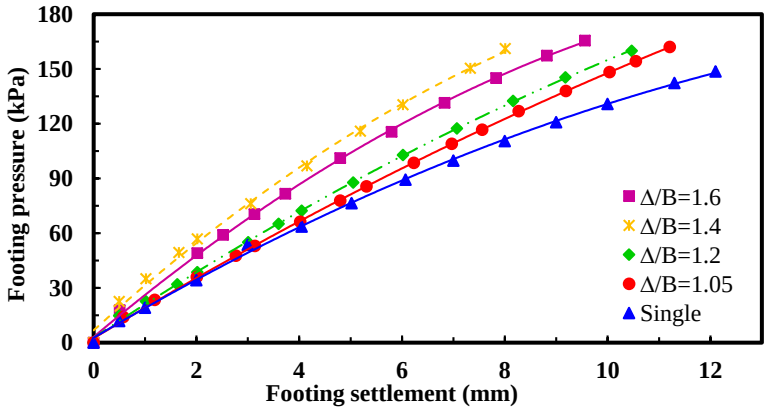

Fig. 7 Load-settlement variation from LVDT for single and interfering footings on geocell-reinforced sand for N=1 and u/B=0.1 at various Δ/B values

settlements corresponding to S/B=10%, as seen in Fig. 6. As the distance between two geocell layers increased, the effect of the second geocell layer decreased. As a result, $(\frac{h}{B})_{cr}$ for geocell and geogrid reinforcements are 0.1 and 0.3, respectively. Thus, it is recommended using this ratio to reach better performance and efficiency of reinforced soils supporting twin footings. Similar observations were also made by Ghazavi and Lavasan (2008) for twin square footings resting on geogrid reinforced soils.

5.2.2 The effect of spacing ratio of the footings

Another series of model tests was performed to study the effect of interference on the behavior of geocell-reinforced sand supported twin footings with changing center to center distance of the footings. Fig. 7 showing measurements from LVDT demonstrates that the maximum bearing pressure of footings on geocell-reinforced soil is achieved when Δ/B is almost 1.4. It can be attributed to the more overlap and interaction between footings at smaller

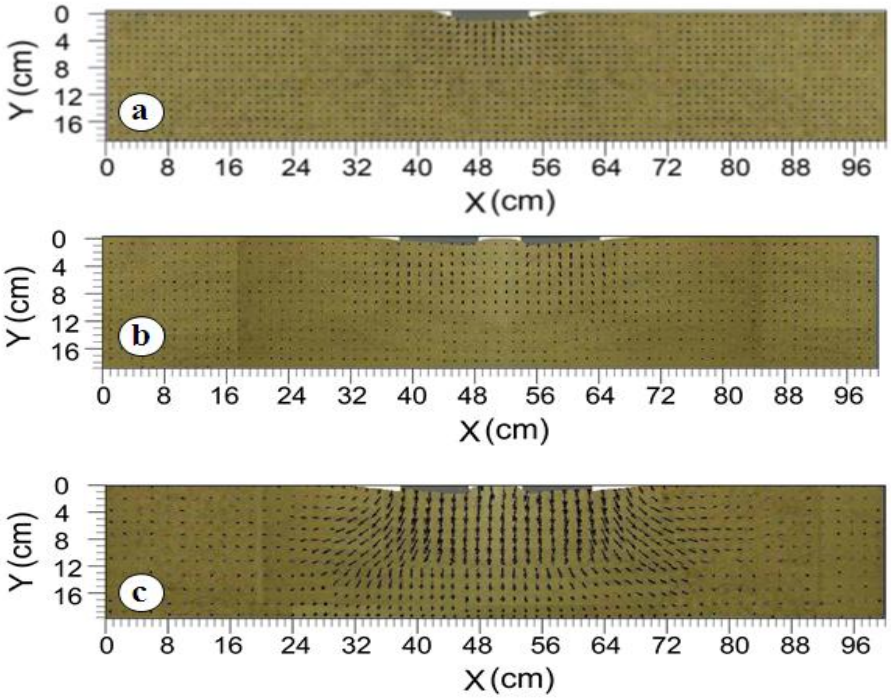

Fig. 8 Deformation pattern in soil under single footing and twin footings on geo-reinforced sand from PIV analysis for: (a) single footing, geocell, N=1, u/B=0.1, (b) twin footings, geocell, Δ/B=1.6, u/B=0.1, N=1 and (c) twin footings, geogrid, Δ/B=1.6, u/B=0.3, N=1

spacing. The amount of Δ/B=1.4 can be named critical spacing in which this value is close to those reported from other studies (Mabrouki *et al*. 2010, Lavasan *et al*. 2018).

The maximum interference behavior of twin footings is attributed to the so-called "blocking effect" reported by Stuart (1962). In this situation, the soil between adjacent foundations forms a reverse arch which moves down with the footings as the load is applied. When Δ/B =1.4-1.6, the maximum bearing capacity is achieved and the pair of footings act as a single foundation. Thus, the critical value of spacing ratio for the twin strip footings will be about $(\Delta/B)_{cr}$=1.4. This amount depends on footing width and soil characteristics (Ghazavi and Fazeli Dehkordi 2021).

5.3 PIV results

5.3.1 Analysis of soil deformation patterns

PIV technique was used to evaluate the effect of interference on the load-settlement of twin footings on geo-reinforced soil during loading. Fig. 8 illustrates that the deformation of reinforced sand under single footing is markedly smaller than that of the same situation for twin footings at the same embedded depth. Moreover, as seen, the length of the vectors significantly reduces with moving downward from the footing bottom. Meanwhile, the vertical soil movement increases by declining the distance of twin footings and this movement is larger than the soil movement beneath single isolated footing. This event supports the argument that the interaction of the pressure bubbles affects the settlement of the footings and soil particles' vertical displacement, located among the footings.

The sand surface deformation between twin footings which showed the blocking effect was like an upright arch shape. More arch formation and moving downward for geogrid reinforced sand bed occurs than geocell reinforced sand bed.

The settlement of all strip footings has been measured using data analysis from LVDT and PIV to monitor the locations of soil particles in the horizontal and vertical directions. The soil vertical displacement values under footings in the X and Y directions (in which X and Y denote the horizontal distance from the axis of symmetry and the depth below the footing, respectively) can be measured. Thus, the continuous vertical displacements at different depths and distances from the footing system symmetry axis were examined for further experiments. At a given foundation settlement, the vertical displacement of soil particles decreases as the depth increases from the footing bottom. In addition, at greater depths, the vertical displacement of soil particles is much lower than those achieved from the foundations. The characteristics of loose sandy soil caused it to compact below the footing when applied pressure increased.

Fig. 9 also shows that at a certain depth, with increasing the horizontal distance from the center of the foundation, the vertical displacement of soil particles becomes lower than the foundation settlement. The influence of interference on the settlement of twin footings rested on geo-reinforced sand can also be observed in Fig. 9. With reducing the distance between twin strip footings to Δ/B=1.2, 1.4, and 1.6, the vertical displacement of soil particles increases. The vertical displacement of soil particles between two footings is approximately equal to

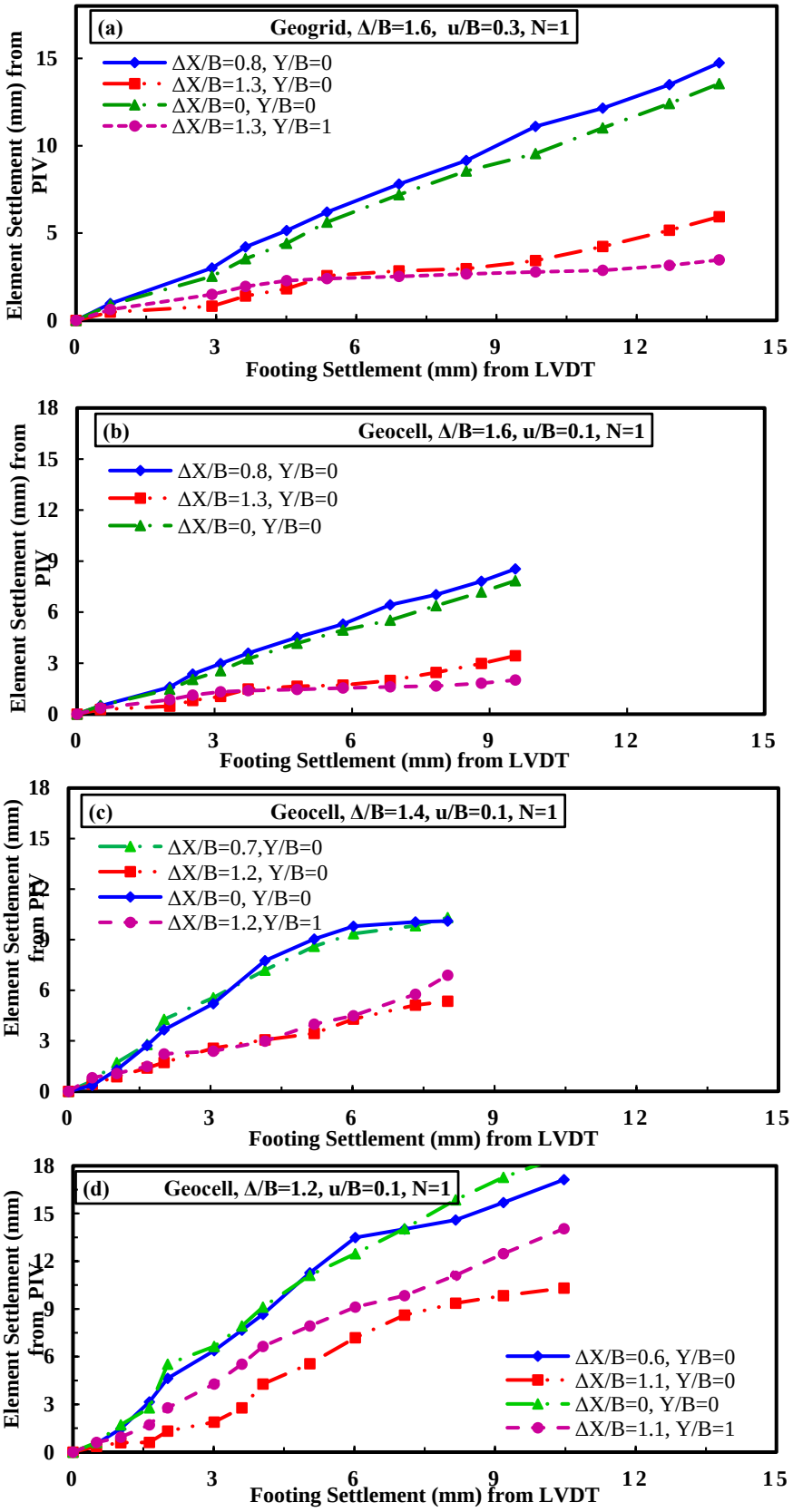

Fig. 9 Comparison between settlements measured of soil particles using PIV and foundations settlement from LVDT for various *X*/*B*, *Y*/*B* and *Δ*/*B* for: (a) geogrid, *Δ*/*B*=1.4, (b) geocell, *Δ*/*B*=1.6, (c) geocell, *Δ*/*B*=1.4 and (d) geocell, *Δ*/*B*=1.2

those achieved from the center of two footings. As seen, the blocking effects that indicate the effect of the footing interference caused twin strip footings to have the same function as a single strip footing (Stuart 1962). On the other

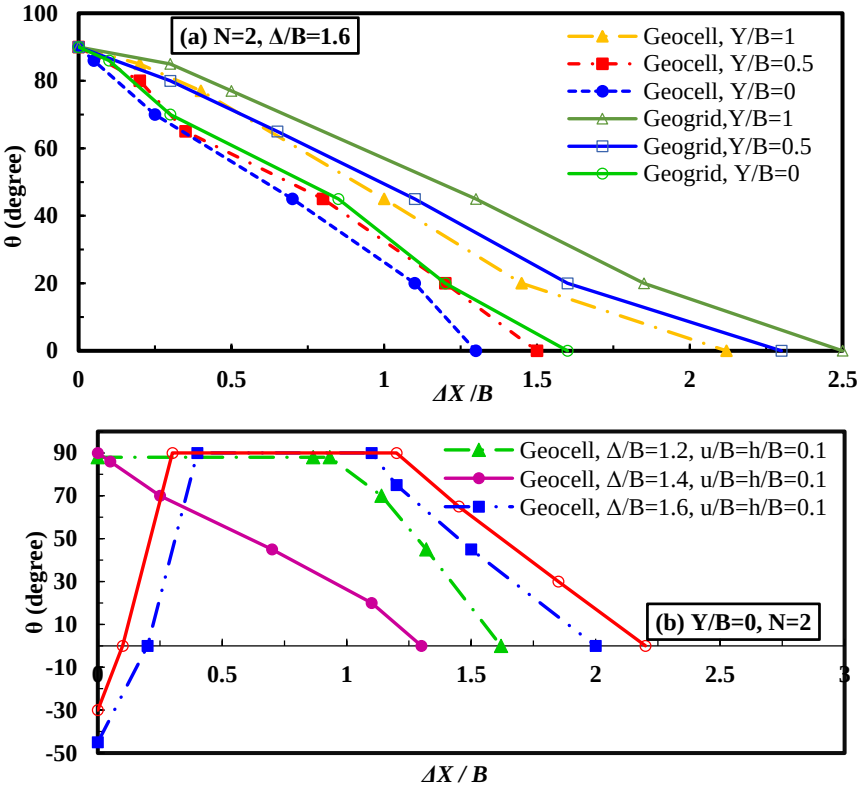

Fig. 10 Vector angles of soil particles toward the horizontal direction for twin footings at various for: (a) Δ/B and (b) Y/B

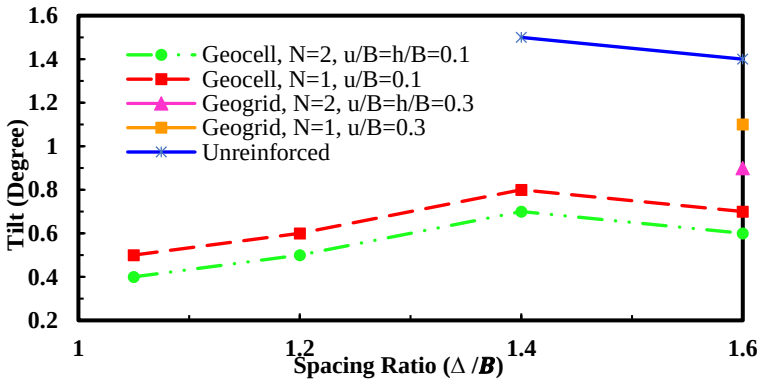

Fig. 11 Variation in footing tilt versus spacing ratio for interfering strip footings on unreinforced and geo-reinforced sand

hand, the blocked soil between footings moves down at the same time with soil particles below footings.

The displacement vectors are used to investigate the soil flow under footings. The soil particles located farther from the footings do not move but the displacement vectors become larger as they approach the footings. The displacement vector angles of soil particles relative to the horizontal direction at various depths around the foundation are shown in Fig. 10(a). As seen, the maximum angle of vectors occurs under the footings. The maximum angle value is observed at the center of the foundation where the force is applied. When moving away from the center, this value decreases. According to Fig. 10(b), twin footings behave like a single footing with a width of $B+\Delta$ when Δ/B=1.2 and 1.4. It underlies the vector angles between footings to be almost constant. For Δ/B=1.6, the effect of interference diminishes compared with Δ/B=1.2 and 1.4. Then, by moving away from the center of each footing to the area between footings, the vector angles decrease.

At $\Delta X \cong 2.5$, the angle value reaches zero for geogrid-reinforced soil, but for geocell-reinforced soil, this reaches zero at $\Delta X \cong 2$. Therefore, it is clear that the length of the influenced surface (ΔX) for geogrid is larger than that of geocell. This may be attributed to further confinement in the geocell-reinforced soil than geogrid-reinforced soil under footings.

5.3.2 Tilt of interfering footings

The tilt of the twin foundations was computed by considering the difference between the two opposite vertical

displacements in each direction. The vertical displacement was deliberated by the soil vertical displacement values from PIV results. The interfering footings-tilt points at various spacing ratios have been presented in Fig. 11.

The occurrence of interfering underlies the tilt of the footings subjected to a vertical centric load (Lavasan *et al*. 2012, Fazeli Dehkordi *et al*. 2019b). From PIV results, an asymmetry in the deformation of the soil surface around each footing could be observed. The tilting was increased when twin strip footings were located at closer spacing. The magnitude of the tilt is about 3˚for unreinforced soil. The maximum tilt occurred when the displacement vectors became the largest in the zone between twin footings (Δ/B=1.4). On the other hand, the maximum footing tilt takes place at critical spacing ratio.

As can be seen in Fig. 11, the magnitude of the footing tilts decreases in geo-reinforced soil. The tilt direction of the footings is not reversed for reinforced soil, and it is different from the results achieved from another study (Lavasan *et al*. 2012). Because in this study, reinforcements covered the entire subgrade and the tensile and shear strength of the reinforcements are the same in all regions. Reinforcing soil with one and two geocell layers reduces the tilt of twin footings by about 70% and 80%, respectively. For twin footings on geogrid-reinforced soil, these values account for about 50% and 60%, respectively. The results show that geocell is more effective than geogrid to reduce the tilt of footings. Actually, geocell have greater membrane and shear stiffness than geogrid and it prevents moving soil in the zones subjected to larger pressures.

5.3.3 Shear strain distribution in soil under twin footings

The shear strain distributions in the soil due to footing loading were measured with PIV analysis and shown in Fig. 12 for individual and two neighboring footings. The maximum strain was created in the upper reinforcement layer only below strip footings. The shear strains appear superficially in the unreinforced samples, and form as shear failure wedges (Figs. 12(a)-12(c)). For reinforced soil, deeper shear strain develops into the soil without any trace of shear failure wedge (Figs. 12(d)-12(f)). Because the reinforcement resembles a relatively rigid slab and transfers the applied load into a deeper zone thus, the shear strain is significantly reduced on the surface. Unlike the zone of pressure bulb for the unreinforced test, a relatively uniform pressure bulb is observed for the reinforced case. As observed in Figs. 12(d)-12(f), the size of highly deformed zones was measured in both geo-reinforced and unreinforced beds to compare their dimensions in single and twin footings.

The depth of zones in geocell-reinforced sand increases to about 2 times of the depth of zones in unreinforced sand. However, the width of zones in geocell-reinforced sand at the ground surface decreases to 50 percent of that of zones in unreinforced sand at the same place. This could be attributed to the high degree of interlocking and improved shear strength parameters of geocell-reinforced soil. Also, a comparison between shear strain distribution in geocell-reinforced sand and geogrid-reinforced sand shows that the use of geocell reinforcement was beneficial. The width of zones in geocell-reinforced sand at the ground surface decreases to 70 percent of that of zones in geogrid-reinforced sand, as observed in Figs. 12(f) and 12(g). As a result, the reinforcements transfer developed shear stresses beneath the loaded area to adjacent stable soil zones, resulting in a deeper failure surface. Therefore, reinforcing soil causes a substantial decrease in magnitude of deformations.

According to Fig. 12(b) and 12(c), when the distance between twin footings decreases, the size of radial shear zone around the interior footing edge reduces continuously as compared to its size around the exterior footing edge. The results from the mechanism provide a good comparison with the theory of Stuart (1962). As a consequence of this phenomenon, a unique failure zone is created with a larger size beneath the system (Lavasan and Ghazavi 2016). It means for the twin footings, deeper shear strain distribution in soil is created compared to individual footing because of the blocking effect of the soil between twin footings. The depth of shear strains in twin footings at Δ/B=1.6 and 1.4 on geocell-reinforced sand are approximately 1.4 and 1.8 times those for individual footing, respectively. In addition, the footing interference decreases with increasing the footing spacing and shear strain contours become distant from each other and separate gently. Figs. 12(b) and 12(c) supports this idea that the interference declined the size of heaved zones around the footings. On the other hand, the geocell reinforced soil is superior compared to the geogrid reinforced soil to constrain the size of heave zones around the footing as shown Figs. 12(e)-12(g). Moreover, with decreasing the footing spacing, the settlement increases due to interference effects.

6. Numerical analysis

A numerical study on the effect of pair strip footings on geo-reinforced sand is also conducted using 3-dimensional finite element modeling (FEM) based on the PLAXIS-V.20 program. The geometry used in the numerical modeling was exactly the same as that considered in experiments. 15-node triangular elements were used for the soil and the Mohr-Coulomb failure criterion was used to simulate its failure. Very fine mesh with a refinement was used around the footing in all analyses to represent the stress concentration. The number of elements, mesh size, soil properties and footing dimensions were kept the same in all analyses. Fig. 13 shows the finite element mesh, nodes and geometry of the generated reinforcement in the numerical modeling. The dilation angle was assumed to be zero because the friction angle of the soil was less than 30˚ (Brinkgreve *et al*. 2020). To simulate geocell reinforcement, geogrid elements were used. The shape of geocell cells in the numerical model was similar to those employed in the experiments. The embedment depth and vertical distance between reinforcements was also selected the same as experiments. The footing is represented by an elastic plate element modeled.

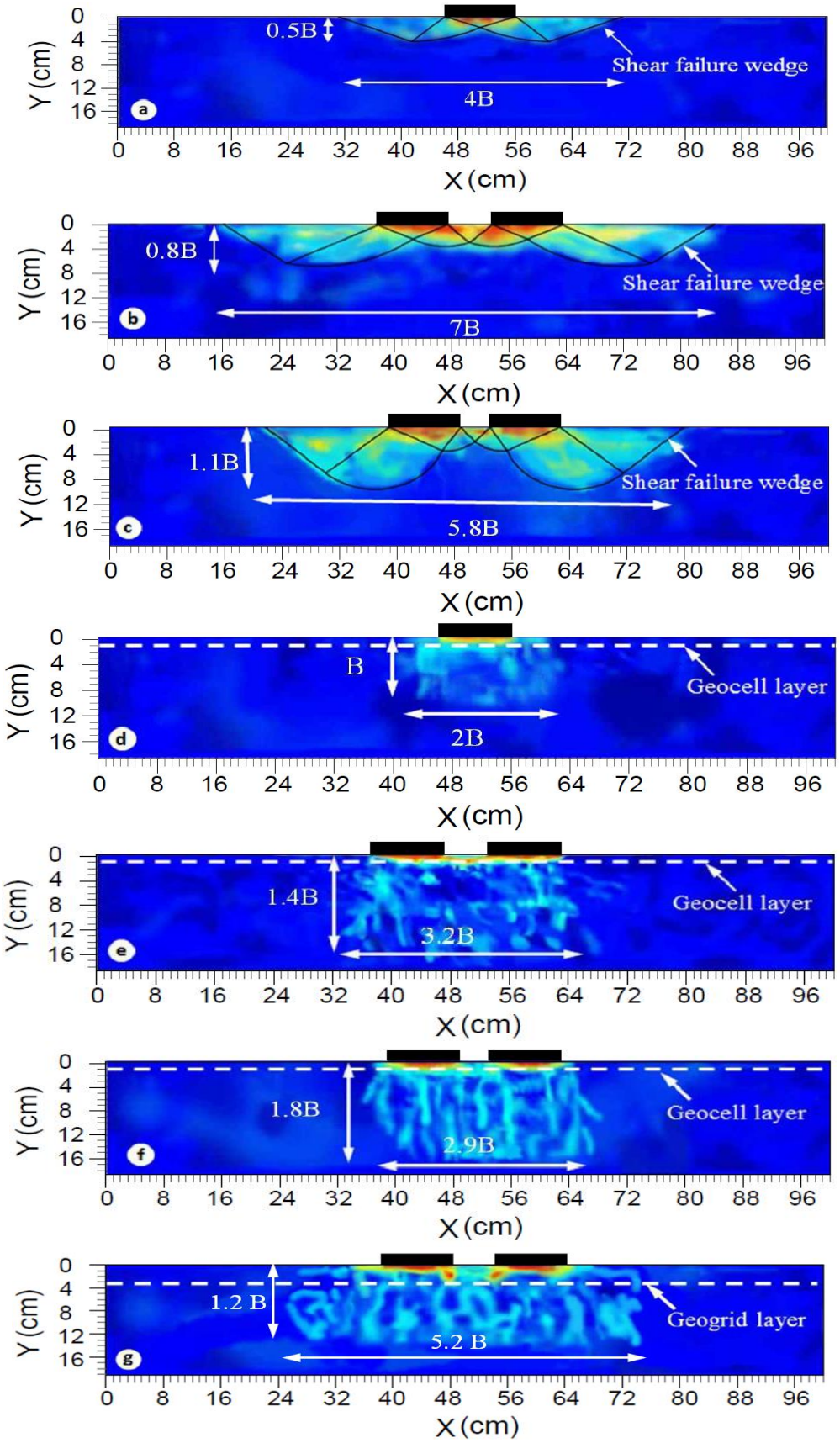

Fig. 12 Shear strain distribution and its dimension in the soil obtained from PIV analysis (a) single footing, unreinforced sand, (b) twin footings, unreinforced sand, Δ/B=1.6, (c) twin footings, unreinforced sand, Δ/B=1.4, (d) single footing, geocell-reinforced sand, u/B=0.1, N=1, (e) twin footings, geocell-reinforced sand, Δ/B=1.6, u/B=0.1, N=1, (f) twin footings, geocell-reinforced sand, Δ/B=1.4, u/B=0.1, N=1, 1 and (g) twin footings, geogrid-reinforced sand, Δ/B=1.6, u/B=0.3, N=1

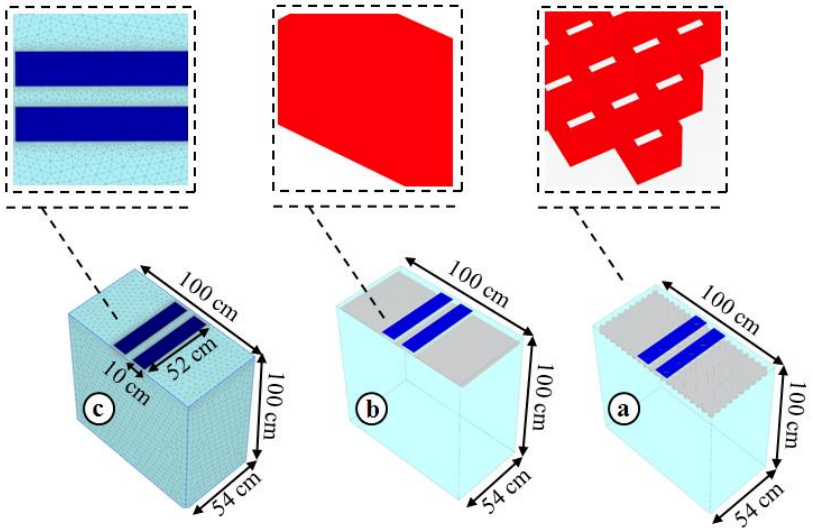

Fig. 13 Diagram showing configuration of footings in PLAXIS program (a) view of geocell-reinforced sand, (b) view of geogrid-reinforced sand and (c) geometry model for analysis of surface vertical condition

Table 4 Parameters used in numerical analyses

Material	Parameter	Value
Sand	Unit weight (kN/m^3)	15.71
	Cohesion (kPa)	4
	Friction angle (φ)	28
	Angle of dilatancy (ψ)	0
	Poisson's ratio	0.3
	Modulus of elasticity (kPa)	20000
	R_{int}*	0.67
Reinforcement	Thickness (mm)	2.2
	Elastic stiffness of geogrid, *EA* (kN/m)	20
Footing (Plate)	Unit weight of footing (kN/m^3)	78
	Modulus of elasticity, *E* (kN/m^2)	2×10^8
	Poisson's ratio	0.3

The analyses were carried out under the displacement-controlled loading, which is a critical indicator for the foundation design. The interface elements between any soil-footing interface with zero physical thickness are assigned by a strength reduction factor of R_{int}=0.67. The parameters used in the numerical analysis are summarized in Table 4.

Fig. 14 shows examples of the total displacement for single and interfering strip footings on geo-reinforced sand. A drastic decline in wide zones in geocell-reinforced sand is observed compared to that due to geogrid-reinforced sand supporting footing. This reflects more benefits of geocell reinforcement to reduce the deformation zone of soil under footings compared with those due to application of geogrid reinforcement. As seen, closely placed footings change twin footing bearing capacity and settlement pattern. It could be concluded that the footings and soil between them behave like a combined system, and then this arrangement moves down upon loading together because of blocking effect. Both numerical analysis and results of PIV technique confirm that blocked soil moves at the same time with footing under loading. Comparing the depth of the influenced zone propagated in the soil under interfering and single footings represents footing interference leads to deeper influenced zones even twice that of single footings. It is emphasized that in this study, numerical analyses were performed on footings on which tests were performed. Thus, it was possible to increase the distance between twin footings up to about 1.6*B* to prevent the effect of boundaries on results. Similar to single isolated footing, for twin footings, the width of influence zone for geocell-reinforced soil is smaller than that for geogrid-reinforced soil. This may be attributed to further confinement which stems from the presence of by a geocell layer under footings.

7. Verifying the results

Fig. 15 indicates the load-displacement curves for some cases considered from the current tests and numerical analysis. The figure clearly shows good agreement in the general behavior trend for both PIV and numerical results. As seen for the reinforced sand at a given load applied to

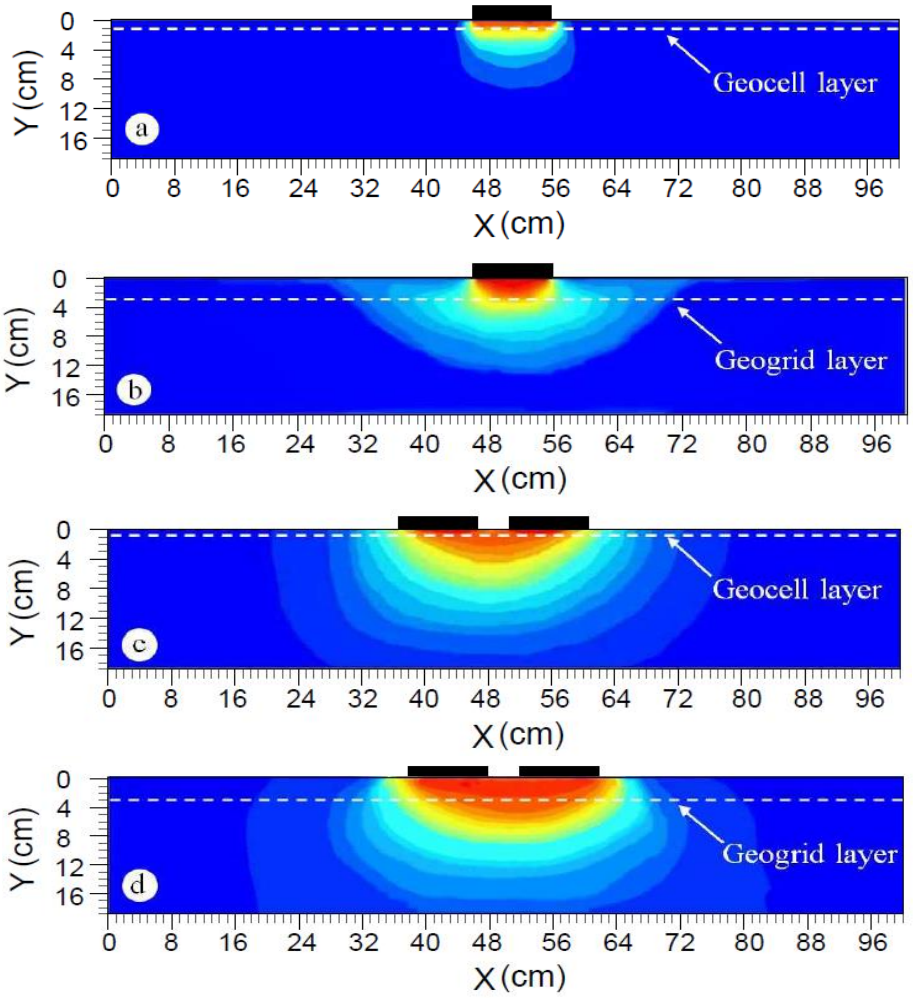

Fig. 14 Section view of the displacement contours obtained from numerical analysis for: (a) single footing on geocell-reinforced soil with N=1, u/B=0.1; (b) single footing on geogrid-reinforced soil with N=1, u/B=0.3, (c) twin footings on geocell-reinforced soil with N=1, Δ/B=1.4, u/B=0.1 and (d) twin footings on geogrid-reinforced soil with N=1, Δ/B=1.4, u/B=0.3

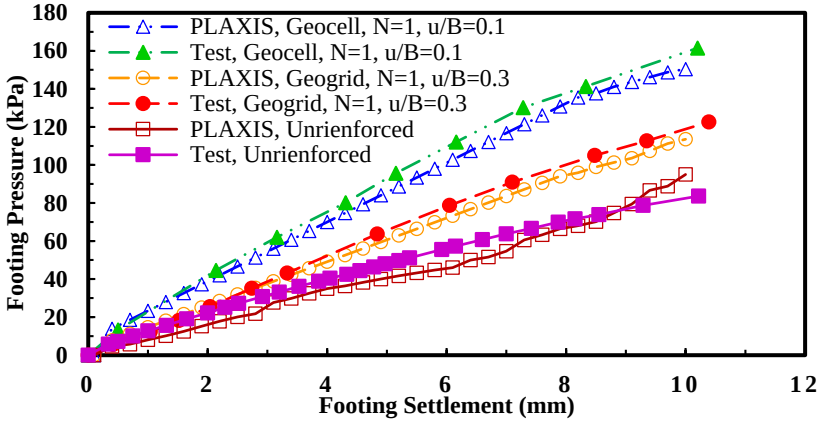

Fig. 15 Comparing PLAXIS and laboratory test results for interfering footings on unreinforced and geo-reinforced sand at Δ/B=1.6

footings, numerical simulation predicts little more settlements than test results which may be attributed to the effect of soil anisotropy in laboratory tests. However, it could be stated that the proposed numerical 3D model is capable of predicting the load-carrying capacity and the settlements of footings on geo-reinforced sand with sufficient accuracy.

In Fig. 16 the vectors of soil deformation in numerical

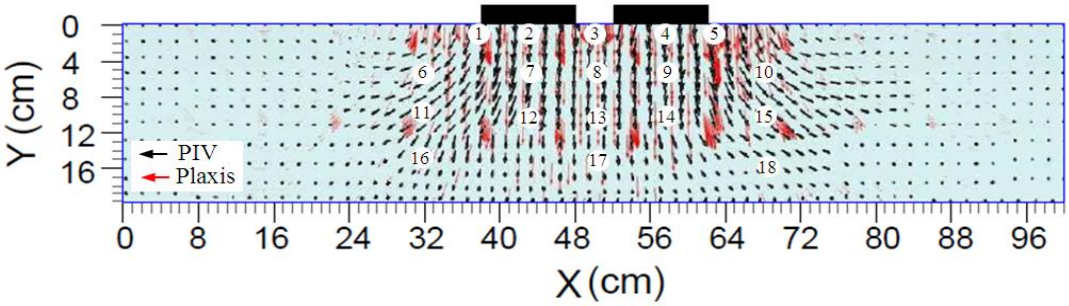

Fig. 16 Deformation pattern in the soil under twin footings on geo-reinforced sand from PLAXIS and PIV at Δ/B=1.4

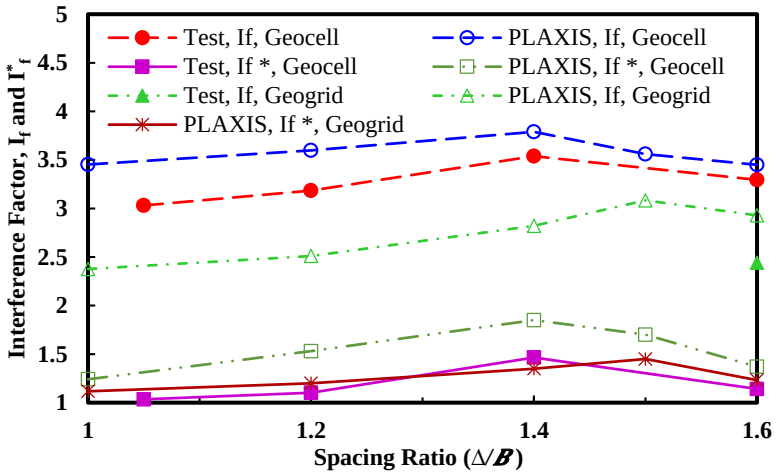

Fig. 17 Comparing PLAXIS and laboratory test results for variation of I_f and I_f^* versus spacing ratio for interfering strip footings on geocell- reinforced sand for N=2, u/B=0.1 and h/B=0.1 and geogrid-reinforced sand for N=2, u/B=0.3 and h/B=0.3

Table 5 Settlements measured of soil particles using PIV and PLAXIS

Point	PLAXIS (mm)	PIV (mm)
1	11	6
2	17	12
3	18	13
4	15	11
5	10	6
6	9	4
7	14	9
8	15	10
9	15	10
10	10	5
11	10	4
12	12	8
13	13	8
14	13	8
15	9	5
16	8	3
17	12	7
18	7	2

modeling were conformed to their obtained from PIV analyses. As seen, there exists a good agreement between the vectors obtained from two analyses, which shows the accuracy of the both analysis. To monitor the values of soil deformation below and between footings, some points were marked in Fig. 16. The settlements of soil particles for each point using PIV and PLAXIS were measured and the results are shown in Table 5. As seen, the maximum difference between the obtained results from two techniques is only 5 mm. The difference could be attributed to assumptions considered in the numerical modeling, such as soil homogeneity. Moreover, slight soil disturbance during preparation or any errors in data measurements can cause this difference.

8. Dimensionless factors

Dimensionless factors are defined here to evaluate the behavior of two neighboring footings on geocell-reinforced sand. These factors were analyzed using obtained load-displacement data from experiments.

According to the literature, to evaluate the influence of interference on the applied pressure of twin strip footings, the following dimensionless factors can be defined as

$$I_f=\frac{q_{int\text{-}N}}{q_{single}} \qquad I_f^*=\frac{q_{int\text{-}N}}{q_{single\text{-}N}} \tag{5}$$

where, q_{int-N} is the ultimate bearing capacity of the

interfering footings on reinforced soil with *N* geocell layers and q_{single} and $q_{single-N}$ represent the ultimate bearing capacities of the same single individual footing on unreinforced and reinforced soil with *N* geocell layers, respectively.

Fig. 17 shows the measured data from LVDT and compares the amount of I_f and I_f^* obtained from tests and FEM for twin footings on geo-reinforced soil. The FEM results indicate that for strip footings on geocell-reinforced sand, the maximum interference effect takes place when Δ/B=1.4, while for geogrid-reinforced sand, this value is almost Δ/B=1.5. The FEM analysis indicates that $I_{f\,\text{maximum}}$ and $I_{f\,\text{maximum}}^*$ values for geocell-reinforced sand is about 25% greater than those for geogrid-reinforced sand at the ultimate settlement ratio. A close agreement between the experimental and numerical trend lines is observed in Fig. 17. As seen, combination positive effects of geocell reinforcement and interference can enhance the footing bearing pressure by approximately 380% at ultimate settlement ratio.

9. Applicability and limitation

Although the present study results can be different with full-scale behavior in general, the overall trend may be similar for scaling of each factor. This research can help to validate the results of numerical models, full-scale or large-scale physical models and centrifuge model tests. Although this research work encourages the beneficial application of soil reinforcement and the influence of interference on the settlement of twin footings, it should be noted that the results are limited to the selected materials, experimental setup geometry, and testing procedure. Previous studies showed that the general trend in small model tests on the reinforced soils could be used to compare the results obtained from large-scale trials (Adams and Collin 1997, Milligan *et al*. 1986). However, the scaling effect is necessary to simulate soil and reinforcement properties to obtain relevant results for practical purposes. Scaling factor in this study is reduced to a particular scale (λ) which shows the prototype base width to the base width of the physical model. On the basis of scaling laws explained above, the results are extrapolated to the prototypical case of the shallow foundations (such as railways, small footings close to each other, the tire contact on the pavement) on the reinforced soil. The plate width used in the current study is 100 mm and assuming the width of strip foundations in the prototype cases is about 250 mm, the scale factor can be deduced as, ($\lambda=\frac{250}{100}=2.5$). On the other hand, the tensile strength of the reinforcements in prototype cases must be λ^2 time's stiffer according to the literature (Langhaar 1951, Buckingham 1914). Given that tensile strength of the geocell used in this study (T_t) equals 6 kN/m, the required tensile strength of the geocell mattress in prototype cases (Tp) is about

$$T_p=T_t\times \lambda^2=6\ \text{kN/m}\times 2.5^2=37.5\ \text{kN/m} \quad (6)$$

In addition, using geocell reinforcement with λ^2 stiffer than the stiffness of the geocell used in this study is possible due to the fact that, maximum tensile strength of geocells available in the market are approximately 35 kN/m which is close to required tensile strength for practice.

It is very important to maintain the soil characteristics same in both physical model and prototype in order to avoid the particle size effect. Thus, the unit weight of the soil must be the same in model and prototype. Although considering the involvement of several complex factors in the performance of reinforced soils, making the exact similarity between the model and prototype is impossible; these results could help in order to design reinforced soils supporting twin footings in practice. Thus, scaling up the factors by considering the accuracy and the nature of the problem should be left to the judgment of the researchers (Fakher and Jones 1996).

10. Conclusions

This paper describes laboratory-scale model tests on a pair of strip footings placed on the geo-reinforced sand beds to show the influence of interference on the load-carrying capacity of the footings. Particle image velocimetry (PIV) was used to monitor the soil deformations beneath and between footings. Numerical modeling is also conducted to verify the experimental results, monitoring failure mechanism and conformity of soil deformation obtained from PIV analysis. The following remarks may be drawn from this study:

The use of both planar (geogrid) and 3-dimensional (geocell) reinforcements caused a significant improvement on the footing load-carrying characteristics of twin strip footings compared to the unreinforced soil bed. The geocell reinforcement offers almost 25% more outstanding performance than geogrid reinforcement at the ultimate settlement ranges.

- The position of reinforcement notably influences the performance of two nearby footings. The critical depth of topmost layer and vertical distance of the geocell layers ($(\frac{u}{B})_{cr}$ and $(\frac{h}{B})_{cr}$) are about 0.1 while those for geogrid layer are 0.3.
- The critical spacing ratio of the twin strip footings $(\Delta/B)_{cr}$ is about 1.5 and 1.4 for geogrid and geocell reinforcement, respectively.
- A combination effect of reinforcement and interference influence enhances the bearing pressure of twin strip footings up to 3.8 and 3.1 for geocell and geogrid reinforcements, respectively compared to the same single footing on the same unreinforced soil bed.
- At a greater depth of soil medium, the vertical displacement of soil particles under loading decreases. The vertical displacement of soil particles for two interacting footings is much lower than the foundation's settlement. With increasing the distance between footings, the vertical displacements of soil particles between footings decline.
- The depth and width of shear strains under twin footings on geocell and geogrid-reinforced sand are almost 1.2 to 2.2 times and 1.6 to 2.6 times those of the same footings on the same unreinforced soil,

respectively, depending on the footings spacing. The depth-influenced zone from shear strains for the twin footings on the geocell-reinforced sand is more profound than those obtained for geogrid-reinforced sand while the width of the influenced zone is smaller.

- The interference causes tilt under vertical centric loads and this effect can be decreased by using reinforcement layers. The geocell reinforcement reduces the footing tilt by 50% more than the geogrid layer for using one and two reinforcement layers.
- The use of two geogrid layers consumes 40% more material than using one geocell layer and the efficiency of one geocell layer is more than using two geogrid layers. This shows the benefits and efficiency of geocell reinforcement.

References

Abu-Farsakh, M.Y., Gu, J., Voyiadjis, G. and Tao, M. (2007), "Numerical parametric study of strip footing on reinforced embankment soils", *Transport. Res. Record*, **2004**(1), 132-140. https://doi.org/10.3141/2004-14.

Adams, M.T. and Collin, J.G. (1997), "Large model spread footing load tests on geosynthetic reinforced soil foundations", *J. Geotech. Geoenviron. Eng.*, **123**(1), 66-72. https://doi.org/10.1061/(ASCE)1090-0241(1997)123:1(66).

Adrian, R.J. (1991), "Particle-imaging techniques for experimental fluid mechanics", *Annu. Rev. Fluid Mech.*, **23**, 261-304. https://doi.org/10.1146/annurev.fl.23.010191.001401.

Alimardani Lavasan, A. and Ghazavi, M. (2012), "Behavior of closely spaced square and circular footings on reinforced sand", *Soils Found.*, **52**(1), 160-167. https://doi.org/10.1016/j.sandf.2012.01.006.

Alimardani Lavasan, A. and Ghazavi, M. (2016), "Failure mechanism and soil deformation pattern of soil beneath interfering square footings", *Int. J. Numer. Method. Civil Eng.*, **1**(2), 48-56. https://doi.org/ 10.29252/nmce.1.2.48.

Alimardani Lavasan, A., Ghazavi, M. and Schanz, T. (2017), "Analysis of interfering circular footings on reinforced soil by physical and numerical approaches considering strain-dependent stiffness", *Int. J. Geomech.*, **17**(11), 4017096-4017096. https://doi.org/10.1061/(ASCE)GM.1943-5622.0000992.

Amar, S., Baguelin, F., Canépa, Y. and Frank, R. (1994), "Experimental study of the settlement of shallow foundations", *Vertical and horizontal deformations of foundations and embankments*, 1602-1610.

Arenson, L.U., Sego, D.C. and Take, W.A. (2007), "Measurement of ice lens growth and soil consolidation during frost penetration using particle image velocimetry (PIV)", *Proceedings of the 60th Canadian Geotechnical Conference*.

Arvin, M.R., Heidari Sooreshjani, M. and Khademhosseini, A. (2021), "Behaviour of geocell-reinforced strip footings on slopes", *Geomech. Geoeng.*, **17**(4), 1-17. https://doi.org/10.1080/17486025.2021.1912404

ASTM D6637 (2011), "Standard test method for determining tensile properties of geogrids by the single or Multi-Rib Tensile Method", *ASTM International*.

ASTM D2487 (2011), "Standard practice for classification of soils for engineering purposes (unified soil classification system)", *ASTM International*.

ASTM D7181 (2011), "Method for consolidated drained triaxial compression test for soils", *ASTM International*.

Biswas, G., Biswas, N. and Ghosh, P. (2018), "Interaction of adjacent strip footings on reinforced soil using upper-bound limit analysis". *Geosynthetics Int.*, **25**(6), 599-611. https://doi.org/10.1680/jgein.18.00020.

Binquet, J. and Lee, L.K. (1975), "Bearing capacity tests on reinforced earth slabs", *J. Geotech. Eng. Div.*, **101**(12), 1241-1255. https://doi.org/10.1061/AJGEB6.0000219.

Boufarh, R., Abbeche, K. and Abdi, A. (2019), "Experimental investigation of interference between adjacent footings on layered cohesionless soil", *Soil Mech. Found. Eng.*, **56**, 128-135.

Braim, K.S., Ahmad, S.N.A.S., Rashid, A.S.A. and Mohamad, H. (2016), "Strip footing settlement on sandy soil due to eccentricty load", *Int. J. Geomate*, **11**, 2741-2746.

Brinkgreve, R.B.J., Swolfs, W.M. and Engin, E. (2020), *Plaxis 2d user's manuals*.

Buckingham, E. (1914), "On physically similar systems; illustrations of the use of dimensional equations", *Phys. Rev.*, **4**, 345-345. https://doi.org/10.1103/PhysRev.4.345.

Bush, D.I., Jenner, C.G. and Bassett, R.H. (1990), "The design and construction of geocell foundation mattresses supporting embankments over soft grounds", *Geotext. Geomembranes*, **9**(1), 83-98. https://doi.org/10.1016/0266-1144(90)90006-X.

Das, B.M. and Larbi-Cherif, S. (1983a), "Bearing capacity of two closely spaced shallow foundations on sand", *Soils Found.*, **23**(1), 1-7. https://doi.org/10.3208/sandf1972.23.1.

Das, B.M. and Larbi-Cherif, S. (1983b), "Ultimate bearing capacity of closely spaced strip foundations", *TRB Transp Res Rec*, **945**, 37-39.

Dash, S.K., Sireesh, S. and Sitharam, T.G. (2003b), "Model studies on circular footing supported on geocell reinforced sand underlain by soft clay", *Geotext. Geomembranes*, **21**(4), 197-219. https://doi.org/10.1016/S0266-1144(03)00017-7.

Dash, S.K., Sireesh, S. and Sitharam, T.G. (2003a), "Behaviour of geocell-reinforced sand beds under circular footing", *P. I. Civil Eng. -Ground Improvement*, **7**(3), 111-115. https://doi.org/10.1680/grim.2003.7.3.111.

Dash, S.K., Krishnaswamy, N.R. and Rajagopal, K. (2001), "Bearing capacity of strip footings supported on geocell-reinforced sand", *Geotext. Geomembranes*, **19**(4), 235-256. https://doi.org/10.1016/S0266-1144(01)00006-1.

Fakher, A. and Jones, C.J. (1996), "Discussion: bearing capacity of rectangular footings on geogrid-reinforced sand", *J. Geotech. Eng.*, **122**(4), 326-327. https://doi.org/10.1061/(ASCE)0733-9410(1996)122:4(326).

Fazeli Dehkordi, P., Karim., U.F.A., Ghazavi, M. and Ganjian, N. (2019a), "Stochastic analysis of the capacity of two parallel footings on a thin sand layer", *P. I. Civil Eng.-Geotech. Eng.*, **172**(4), 355-364. https://doi.org/10.1680/jgeen.18.00094.

Fazeli Dehkordi, P., Ghazavi, M., Ganjian, N. and Karim, U.F.A. (2019b), "Effect of geocell-reinforced sand base on bearing capacity of twin circular footings", *Geosynthetics Int.*, **26**(3), 224-236. https://doi.org/10.1680/jgein.19.00047.

Fazeli Dehkordi, P. and Karim, U.F.A. (2020), "Behaviour of circular footings confined by rigid base and geocell reinforcement", *Arabian J. Geosci.*, **13**, 1-12. https://doi.org/10.1007/s12517-020-06092-1.

Fazeli Dehkordi, P., Ghazavi, M. and Ganjian, N. (2021a), "Evaluation behavior of circular footing located on sand bed reinforced with geocell", *Amirkabir J. Civil Eng.*, **53**(5), 411-414. https://doi.org/10.22060/CEEJ.2020.17159.6479.

Fazeli Dehkordi, P., Ghazavi, M. and Karim, U.F.A. (2021b), "Bearing capacity-relative density behavior of circular footings resting on geocell-reinforced sand", *Eur. J. Environ. Civil Eng.*, **26**(11), 5088-5112. https://doi.org/10.1080/19648189.2021.1884901.

Fazeli Dehkordi, P., Ghazavi, M., Ganjian, N. and Karim, U.F.A. (2021c), "Parametric study from laboratory tests on twin

circular footings on geocell- reinforced sand", *Scientia Iranica, Transaction A, Civil Eng.*, **28**(1), 96-108. https://doi.org/10.24200/sci.2019.51471.2208.

Fazeli Dehkordi, P. (2022), "Assessment behavior of cojointed footings system placed on sands encased by geocell reinforcement: experimental study", *Amirkabir J. Civil Eng.*, **54**(3), 214-214. https://doi.org/10.22060/ceej.2021.19194.7102.

Fazeli Dehkordi, P., Ghazavi, M., Karim, U.F.A., Valinezhad Torghabeh, N. (2023), "Interacting footings on geo-reinforced soils: A state-of-the-art review", *Submitted to Arabian Journal for Science and Engineering* (Under review).

Ghazavi, M. and Alimardani Lavasan, A. (2008), "Interference effect of shallow foundations constructed on sand reinforced with geosynthetics", *Geotext. Geomembranes*, **26**(5), 404-415. https://doi.org/10.1016/j.geotexmem.2008.02.003.

Ghazavi, M. and Fazeli Dehkordi, P. (2021), "Interference influence on behavior of shallow footings constructed on soils, past studies to future forecast: A state-of-the-art review", *Transport. Geotech.*, **27**, 100502-100502. https://doi.org/10.1016/j.trgeo.2020.100502.

Ghazavi, M., Valinezhad Torghabeh, N., Fazeli Dehkordi, P. (2023), "Analysis of twin circular footings on geocell-reinforced bed using response surface method", *Accepted in: International Journal of Geomechanics*.

Ghalehjough, B.K., Akbulut, S. and Çelik, S. (2018), "Effect of particle roundness and morphology on the shear failure mechanism of granular soil under strip footing", *Acta Geotechnica Slovenica*, **15**, 43-53. https://doi.org/10.18690/actageotechslov.15.1.43-53.2018.

Ghosh, P. and Kumar, P. (2009), "Interference effect of two nearby strip footings on reinforced sand", *Contemporary Engineering Sciences*, **2**, 577–592.

Ghosh, P. and Kumar, S. (2011), "Interference effect of two nearby strip surface footings on cohesionless layered soil", *Int. J. Geotech. Eng.*, **5**(1), 87-94. https://doi.org/10.3328/IJGE.2011.05.01.87-94.

Ghosh, P., Basudhar, P.K., Srinivasan, V. and Kunal, K. (2015), "Experimental studies on interference of two angular footings resting on surface of two-layer cohesionless soil deposit", *Int. J. Geotech. Eng.*, **9**(4), 422-433. https://doi.org/10.1179/1939787914Y.0000000080.

Gupta, A., Talha, M. and Seemann, W. (2018), "Free vibration and flexural response of functionally graded plates resting on Winkler-Pasternak elastic foundations using nonpolynomial higher-order shear and nor- mal deformation theory", *Mech. Adv. Mater. Struct.*, **25**(6), 523-538. https://doi.org/10.1080/15376494.2017.1285459.

Han, J., Yang, X.M., Leshchinsky, D. and Parsons, R.L. (2008), "Behavior of geocell-reinforced sand under a vertical load", *J. Transport. Res. Board*, **2045**(1), 95-101. https://doi.org/10.3141/2045-11.

Yang, X., Han, J., Parsons, R. L. and Leshchinsky, D. (2010), "Three-dimensional numerical modeling of single geocell-reinforced sand", *Front. Struct. Civil Eng.*, **4**, 233-240.

Yoo, C. (2001), "Laboratory investigation of bearing capacity behavior of strip footing on geogrid-reinforced sand slope", *Geotext. Geomembranes*, **19**(5), 279-298. https://doi.org/10.1016/S0266-1144(01)00009-7.

Kolbsuzewski, J. (1948), "General investigation of the fundamental factors controlling loose packing of sands", *Proceedings of the the 2nd International Conference on Soil Mechanics and Foundation Engineering*.

Kumar, A. and Saran, S. (2003), "Closely spaced footings on geogrid reinforced sand", *J. Geotech. Geoenviron. Eng.*, **129**(7), 660-664. https://doi.org/10.1061/(ASCE)1090-0241(2003)129:7(660).

Langhaar, J.L. (1951), "Dimensional analysis and theory of models", John Wiley & Sons, New York, NY.

Lavasan, A.A., Ghazavi, M., von Blumenthal, A. and Schanz, T. (2018), "Bearing capacity of interfering strip footings", *J. Geotech. Geoenviron. Eng.*, **144**, 4018003-4018003. https://doi.org/10.1061/(ASCE)GT.1943-5606.0001824.

Mabrouki, A., Benmeddour, D., Frank, R. and Mellas, M. (2010), "Numerical study of the bearing capacity for two interfering strip footings on sands", *Comput. Geotech.*, **37**(4), 431-439. https://doi.org/10.1016/j.compgeo.2009.12.007.

Marandi, S.M. and Javdanian, H. (2012), "Laboratory studies on bearing capacity of strip interfering shallow foundations supported by geogrid-reinforced sand", *Adv. Mater. Res.*, **472**, 1856-1869. https://doi.org/10.4028/www.scientific.net/AMR.472-475.1856.

Matlab. (2007), Computer Software, MathWorks, Natick, MA, USA.

Mei, L., Ni, P., Mei, G. and Zhao, Y. (2021), "Bearing capacity of plane-strain footings under K0 conditions", *Arabian J. Geosci.*, **14**(11), 953. https://doi.org/10.1007/s12517-021-07111-5.

Miyamoto, S. and Miyata, Y. (2020), "Bearing capacity mechanism of geocell reinforced soil foundations", *Transport. Soil Eng. Cold Reg.*, **2**, 3-12. https://doi.org/10.1007/978-981-15-0454-9_1.

Milligan, G.W.E., Fannin, R.J. and Farrar, D.M. (1986), "Model and full-scale tests of granular layers reinforced with a geogrid", *Proceedings of 3rd international conference on geotextiles*.

Naderi, E. and Hataf, N. (2014), "Model testing and numerical investigation of interference effect of closely spaced ring and circular footings on reinforced sand", *Geotext. Geomembranes*, **42**(3), 191-200. https://doi.org/10.1016/j.geotexmem.2013.12.010.

Ni, P., Song, L., Mei, G. and Zhao, Y. (2018), "Predicting excavation-induced settlement for embedded footing: Case study". *Int. J. Geomech.*, **18**(4), 05018001. https://doi.org/10.1061/(ASCE)GM.1943-5622.0001107.

Oliaei, M. and Kouzegaran, S. (2017), "Efficiency of cellular geosynthetics for foundation reinforcement", *Geo- Text. Geomembranes*, **45**(2), 11–22. https://doi.org/10.1016/j.geotexmem.2016.11.001.

O'loughlin, C.D. and Lehane, B.M. (2010), "Nonlinear cone penetration test-based method for predicting footing settlements on sand", *J. Geotech. Geoenviron. Eng.*, **136**(3), 409-416. https://doi.org/10.1061/(ASCE)GT.1943-5606.0000228.

Pokharel, S.K., Han, J., Leshchinsky, D., Parsons, R.L. and Halahmi, I. (2010), "Investigation of factors influencing behavior of single geocell-reinforced bases under static loading", *Geotext. Geomembranes*, **28**(6), 570-578. https://doi.org/10.1016/j.geotexmem.2010.06.002.

Rea, C. and Mitchell, J.K. (1978), "Sand reinforcement using paper grid cells", *ASCE Spring Convention and Exhibit,* Pittsburgh, PA.

Schmüdderich, C., Alimardani Lavasan, A., Tschuchnigg, F. and Wichtmann, T. (2020), "Behavior of nonidentical differently loaded interfering rough footings", *J. Geotech. Geoenviron. Eng.*, **146**(6), 4020041-4020041. https://doi.org/10.1061/(ASCE)GT.1943-5606.0002255.

Schmüdderich, C., Alimardani Lavasan, A. Tschuchnigg, F. and Wichtmann, T. (2020), "Bearing capacity of a strip footing placed next to an existing footing on frictional soil", *Soils Found.*, **60**(1), 229-238. https://doi.org/10.1016/j.sandf.2020.03.002.

Shadmand, A., Ghazavi, M. and Ganjian, N. (2018), "Load-settlement characteristics of large-scale square footing on sand reinforced with opening geocell reinforcement", *Geotext. Geomembranes*, **46**(3), 319-326. https://doi.org/10.1016/j.geotexmem.2018.01.001.

Sitharam, T.G. and Sireesh, S. (2006), "Effects of base geogrid on

geocell-reinforced foundation beds", *Geomech. Geoeng.*, **1**(3), 207-216. https://doi.org/10.1080/17486020600900596.

Srinivasan, V. and Ghosh, P. (2013), "Experimental investigation on interaction problem of two nearby circular footings on layered cohesionless soil", *Geomech. Geoeng.*, **8**(2), 97-106. https://doi.org/10.1080/17486025.2012.695401.

Srokosz, P.E., Bujko, M., Bocheńska, M. and Ossowski, R. (2021), "Optical flow method for measuring deformation of soil specimen subjected to torsional shearing", *Measurement*, **174**, 109064-109064. https://doi.org/10.1016/j.measurement.2021.109064.

Stuart, J.G. (1962), "Interference between foundations, with special reference to surface footings in sand", *Geotechnique*, **12**(1), 15-22. https://doi.org/10.1680/geot.1962.12.1.15.

Vesic, A.S. (1973), "Analysis of ultimate loads of shallow foundation", *J. Soil Mech. Found. Div. ASCE*, **99**(1), 45-73. https://doi.org/10.1061/JSFEAQ.0001846.

White, D.J. and Take, W.A. (2002), *GeoPIV: Particle Image Velocimetry (PIV) software for use in geotechnical testing*.

White, D.J., Take, W.A. and Bolton, M.D. (2003), "Soil deformation measurement using particle image velocimetry (PIV) and photogrammetry". *Geotechnique*, **53**(7), 619-632. https://doi.org/10.1680/geot.2003.53.7.619.

GC